Stability of voids formed in cavities at liquid-solid interfaces

by

Jeffrey W. Bullard
Building and Fire Research Laboratory
National Institute of Standards and Technology
Gaithersburg, MD 20899 USA

Reprinted from Journal of Colloid and Interface Science, Vol. 276, No. 1, pp. 188-196, 2004.

NIST
National Institute of Standards and Technology
Technology Administration, U.S. Department of Commerce

Available online at www.sciencedirect.com
SCIENCE DIRECT®
Journal of Colloid and Interface Science 276 (2004) 188–196
JOURNAL OF Colloid and Interface Science
www.elsevier.com/locate/jcis

Stability of voids formed in cavities at liquid–solid interfaces

Jeffrey W. Bullard

National Institute of Standards and Technology, Materials and Construction Research Division, Gaithersburg, MD, USA

Received 10 November 2003; accepted 11 March 2004

Available online 16 April 2004

Abstract

A thermodynamic model is developed of the free energy of gas-filled voids formed within cavities on solid surfaces covered by a liquid. Capillary effects are assumed to be the only important contributions to the free energy, and expressions are derived for the free energy of the system as a function of the void size, the relative surface free energy densities involved, and the geometry of the cavity. The results of the model are (1) construction of a stability diagram that maps the most stable void configuration versus the wetting properties of the various solid surfaces involved, and (2) rough estimates of the work required to liberate a void of a given size and position. The model can give qualitative insight into the stability of coating defects on uneven surfaces, and also can be used to prescribe possible surface treatments for reducing the work required to remove voids from the system.

Keywords: Interfaces; Wetting; Thermodynamic modeling; Air voids

1. Introduction

The rapid covering of a solid surface by a liquid is an event common to diverse processes in nature, science, engineering, and medicine. Some examples from manufacturing include processes such as investment casting, electroplating, cleaning, dip coating, spin coating, painting, screen printing, and production of powder slurries. In the field of medicine, examples include the flow of liquids into syringes and through intravenous feeding tubes. By any of these processes, gas may become trapped as isolated pockets, or voids, at liquid–solid surfaces. The number and size of the voids that form depend both on the details of the liquid flow and on the properties of the solid surface, such as its roughness and its tendency to be wet by the liquid. In coating or casting applications, voids that are not removed can result in defects that compromise the adhesion, electrical properties, surface finish, and durability of the product.

Conditions for the initial formation of a void are especially favorable at reentrant features of a rough surface, such as pinhole defects in films, pits and scratches formed by grinding, and even intentional cavities formed by a prior photolithographic or stamping procedure. Flow of liquid can cover such features before the gas can escape, especially if the solid surface is lyophobic. This phenomenon is particularly prevalent, for example, when electrolytically depositing metals into small cavities (≈50 μm diameter) like those formed in photoresist masks for patterning electrical circuits. For such geometries a commonly observed defect is a lens-shaped depression in the deposited metal, as illustrated in Fig. 1. These depressions indicate regions of low current where a bubble prevented adequate liquid contact.

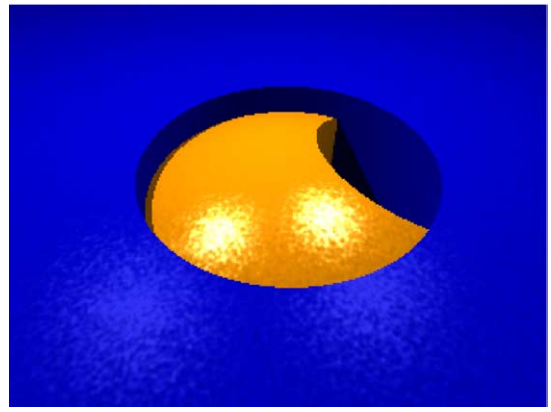

Fig. 1. Illustration of electroplating defect caused by gas-filled voids trapped in recessed cavities.

E-mail address: jeffrey.bullard@nist.gov.

0021-9797/$ – see front matter
doi:10.1016/j.jcis.2004.03.054

Given the negative impact that gas-filled voids have on many processes, it is desirable to find ways either to prevent their formation or to expedite their removal from the system once they have formed. In situations where it is not feasible either to modify the way in which liquid is introduced at the surface or to chemically modify the surfaces, the formation of surface voids may be unavoidable. In many of these systems, voids persist because they are thermodynamically stable. For such systems, voids can be removed only by supplying work, such as mechanical vibration or impact in their vicinity.

This paper analyzes systems in which voids may be trapped in low-energy configurations. A thermodynamic model is presented of a gas-filled void at an idealized reentrant surface feature, and the model is used to calculate the most stable void configuration (including the possibility of the void being liberated from the surface). The approach is similar to that used by Chatain et al. [1] to analyze the thermodynamically stable shapes of two-phase systems enclosed within a cubic cavity. By calculating the free energy of the stable configuration relative to that of a liberated void of the same size, the minimum work required to release the void is predicted. The idealized model has the benefits of being analytically tractable and of leading to insights that should be qualitatively valid for real systems. In fact, as shown in Section 3, even the quantitative predictions of the work required to remove a void are expected to be good approximations that can be used to help design procedures for removing these types of defects.

2. Model description

In this section, the basic model is described in some detail, including the primary assumptions that are used throughout. A two-dimensional model simplifies the mathematical details, and is therefore used for most of the calculations. However, because differences between wetting phenomena in 2-D and 3-D are often significant, a more restricted 3-D model is also developed later in this section as a check on the 2-D results.

2.1. 2-D model system

The basic 2-D model is shown in Fig. 2. It consists of a chemically homogeneous liquid (denoted as L) partially filling a reentrant surface feature. The remainder of the cavity is assumed to be filled with a gas (denoted G). The liquid is assumed to provide a thermal reservoir sufficient to keep the entire system isothermal. Furthermore, the liquid and external atmosphere with which it is in contact are assumed to provide a fixed hydrostatic pressure. As long as the pressure remains fixed, it is a good approximation to take the molar volume of the void to be constant also. The reentrant surface feature is a cavity having width D and depth h. Typical dimensions of D and h are often 10 to 1000 μm in engineering applications. For greater generality, and because of the close resemblance to features found in, for example, selective electrodeposition processes, the base of the cavity (denoted B) is assumed to have different wetting properties than the walls (denoted W). To avoid the complication of appreciable gas solubility or any chemical reactions, the liquid, solids, and gas are assumed to be mutually inert.

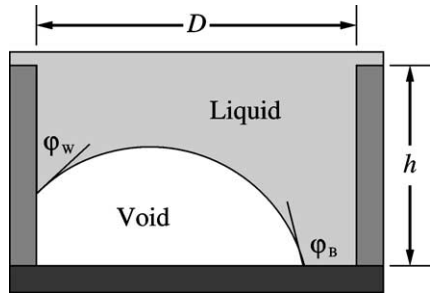

Fig. 2. A schematic of the 2-D void model.

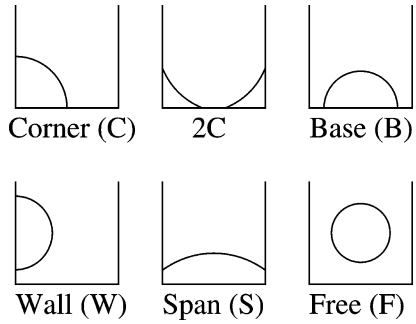

Fig. 3. Different configurations of a void in a surface cavity.

The free energy of the system clearly should depend on the shape and location of the void within the cavity. The possible distinct configurations that a void of a specified volume[1] may adopt are shown in Fig. 3 along with a name and one-letter symbol by which each configuration will be denoted throughout this analysis. In principle, a volume of gas could be partitioned into multiple voids of different sizes, such as one void in each corner or one void at the wall and another at the base. However, as shown in Appendix B, the only circumstance for the system at hand in which this can happen is that for which the interface between the void and the liquid is convex when viewed from within the void. Such a condition is possible geometrically only for the corner configuration, and so we also consider a configuration, labeled as "2C" in Fig. 3, in which two voids having equal volumes form, one at each corner. By calculating the free energy of each configuration at constant void volume, subject to the geometric constraints, the most stable configuration may be determined.

[1] Strictly speaking, "volume" is really an area in 2-D, but for purposed of clarity we will continue to refer to space in 2-D as having volume and to interfaces in 2-D as having area.

Because the gas is assumed to have fixed molar volume and temperature, the free energy, F, written as a function of temperature and all other extensive variables, represents the thermodynamic potential governing equilibrium and stability. We will ignore the presence of body forces arising from gravitational,[2] electrostatic, or centrifugal fields. For constant temperature, void volume and molar content, the bulk contributions to the free energy are invariant and may be subtracted from the true free energy without further loss of generality. We denote the four different types of materials by single capital letters as follows: B = base, W = wall, L = liquid, and G = gas. The area of the interface separating two phases i and j will then be denoted as A_{ij}. With this notation, the free energy may be written as [2,3]

$$\begin{aligned} F &= \tilde{F}(A_{\mathrm{BG}}, A_{\mathrm{BL}}, A_{\mathrm{WG}}, A_{\mathrm{WL}}, A_{\mathrm{LG}}) \\ &= \int_{A_{\mathrm{BG}}} \gamma_{\mathrm{BG}}\, dA_{\mathrm{BG}} + \int_{A_{\mathrm{BL}}} \gamma_{\mathrm{BL}}\, dA_{\mathrm{BL}} \\ &\quad + \int_{A_{\mathrm{WG}}} \gamma_{\mathrm{WG}}\, dA_{\mathrm{WG}} + \int_{A_{\mathrm{WL}}} \gamma_{\mathrm{WL}}\, dA_{\mathrm{WL}} \\ &\quad + \int_{A_{\mathrm{LG}}} \gamma_{\mathrm{LG}}\, dA_{\mathrm{LG}}, \end{aligned} \tag{1}$$

where, for example, A_{BG} is the total area of surface separating the base (B) and gas (G), and

$$\gamma_{\mathrm{BG}} \equiv \left(\frac{\partial \tilde{F}}{\partial A_{\mathrm{BG}}}\right).$$

Fig. 2 shows that $A_{\mathrm{BL}} = D - A_{\mathrm{BG}}$ and $A_{\mathrm{WL}} = 2h - A_{\mathrm{WG}}$. Also, only the differences in free energies of the various configurations are relevant. We therefore subtract from Eq. (1) the constant terms $\gamma_{\mathrm{BL}} D$ and $2\gamma_{\mathrm{WL}} h$, integrate term by term, and normalize by γ_{LG}:

$$\begin{aligned} \Gamma &\equiv \frac{F - \gamma_{\mathrm{BL}} D - 2\gamma_{\mathrm{WL}} h}{\gamma_{\mathrm{LG}}} \\ &= (g_{\mathrm{BG}} - g_{\mathrm{BL}}) A_{\mathrm{BG}} + (g_{\mathrm{WG}} - g_{\mathrm{WL}}) A_{\mathrm{WG}} + A_{\mathrm{LG}}, \end{aligned} \tag{2}$$

where $g_{ij} \equiv \gamma_{ij}/\gamma_{\mathrm{LG}}$.

It can be shown, by minimization of free energy [4–6], that at equilibrium the liquid/gas interface must assume a shape having convex mean curvature.

$$\Delta P = \gamma_{\mathrm{LG}} \kappa,$$

that at equilibrium the liquid/gas interface must assume a shape with constant mean curvature. A wide variety of surface shapes with constant mean curvature, so-called minimal surfaces, can be embedded in three dimensions. However, in 2-D the only constant-curvature surface possible is an arc of a circle. Furthermore, provided that both the walls and base of the cavity are essentially rigid solids, minimization of free energy can be shown to require [7] that the geometry satisfy Young's equation [8],

$$g_{\mathrm{BG}} - g_{\mathrm{BL}} = \cos\phi_{\mathrm{B}}, \tag{3}$$

$$g_{\mathrm{WG}} - g_{\mathrm{WL}} = \cos\phi_{\mathrm{W}}, \tag{4}$$

where ϕ_{B} and ϕ_{W} are the thermodynamic contact angles at the base and wall, respectively (see Fig. 2). Therefore, we may simplify Eq. (2) to

$$\Gamma = A_{\mathrm{BG}} \cos\phi_{\mathrm{B}} + A_{\mathrm{WG}} \cos\phi_{\mathrm{W}} + A_{\mathrm{LG}}. \tag{5}$$

The constitutive variables for the problem at hand are the void volume, V, and the thermodynamic contact angles ϕ_{B} and ϕ_{W}. Therefore we must express, for each configuration, the surface areas A_{ij} in Eq. (5) as explicit functions of these variables. The mathematics are straightforward but tedious and will not be reproduced here. Briefly, the areas are written in Table 1 as functions of the interface radius of curvature, R and then $R(V, \phi_{\mathrm{B}}, \phi_{\mathrm{W}})$ is derived using trigonometry and catalogued in Table 2. An example derivation for the base configuration is given in Appendix A.

Comparison of the free energies for various values of the constitutive variables will establish the global equilibrium configurations of the void as well as the relative work required to liberate the void to the bulk liquid. However, in addition to these free energy considerations, each void configuration can exist only within certain geometric constraints. These constraints are of two types: (1) upper bounds on the linear dimensions of the void, above which the void impinges on another boundary of the cavity; (2) for the C and 2C configurations, the requirement that the liquid–gas interface have constant curvature implies certain inequality relationships between ϕ_{W} and ϕ_{B}. The constraints are catalogued in Appendix C.

Evaluation of stable void configurations in the 2-D model is presented in the Discussion section. But fxfirst, we establish a restricted 3-D model that will be useful for comparison to the 2-D results.

2.2. Three-dimensional model system

For arbitrary values of ϕ_{B} and ϕ_{W}, a 3-D analog to the system depicted in Fig. 2 is difficult to analyze because of the more complex geometries that must be evaluated to determine the volume and areas of the different interfaces. However, the situation simplifies considerably if we assume that $\phi_{\mathrm{W}} = \pi/2$ (i.e., $\gamma_{\mathrm{WG}} = \gamma_{\mathrm{WL}}$). And because we are interested mainly in identifying qualitative differences between the more artificial 2-D system and the 3-D system, we will accept that restriction for the 3-D model. The void will be assumed to reside in a tetragonal cavity (i.e., all walls of equal length D but $D \neq h$). Also, because the walls and base are all mutually orthogonal, the condition that $\phi_{\mathrm{W}} = \pi/2$ makes the problem mathematically identical to that of an axisymmetric

[2] For large voids, buoyancy forces should be considered because they become increasingly important, relative to capillary effects, as the surface/volume ratio decreases. However, for small voids (≈100 μm effective diameter), it is an excellent approximation to ignore gravity.

Table 1
The area of each type of interface as a function of R, ϕ_W, and ϕ_B for each configuration shown in Fig. 3

Configuration	A_{BG}	A_{WG}	A_{LG}
Corner (C)			
$(\phi_W + \phi_B \neq 3\pi/2)$	$R(\cos\phi_W + \sin\phi_B)$	$R(\sin\phi_W + \cos\phi_B)$	$R\left(\frac{3\pi}{2} - \phi_W - \phi_B\right)$
$(\phi_W + \phi_B = 3\pi/2)$	$\sqrt{\frac{2V\cos\phi_B}{\cos\phi_W}}$	$\sqrt{\frac{2V\cos\phi_W}{\cos\phi_B}}$	$\sqrt{\frac{2V}{\cos\phi_B\cos\phi_W}}$
Two-corner (2C)			
$(\phi_W + \phi_B \neq 3\pi/2)$	$2R(\cos\phi_W + \sin\phi_B)$	$2R(\sin\phi_W + \cos\phi_B)$	$2R\left(\frac{3\pi}{2} - \phi_W - \phi_B\right)$
$(\phi_W + \phi_B = 3\pi/2)$	$\sqrt{\frac{V\cos\phi_B}{\cos\phi_W}}$	$\sqrt{\frac{V\cos\phi_W}{\cos\phi_B}}$	$\sqrt{\frac{V}{\cos\phi_B\cos\phi_W}}$
Wall (W)	0	$2R\sin\phi_W$	$2R(\pi - \phi_W)$
Base (B)	$2R\sin\phi_B$	0	$2R(\pi - \phi_B)$
Span (S)			
$V \leqslant V_c$	D	$2h_p$	$2R\left(\frac{\pi}{2} - \phi_W\right)$
$V > V_c$	D	$2h - D + 2R\sin\phi_W$	$2R(\pi - \phi_W)$
Free (F)	0	0	$2\pi R$

For the C and 2C configurations, $R \to \infty$ as $\phi_W + \phi_B \to 3\pi/2$, so the void assumes the shape of a right triangle and the areas are functions of V. For the span configuration, h_p is the height above the base of the triple junction formed at each wall.

Table 2
R as a function of V, ϕ_W and ϕ_B for the configurations shown in Fig. 3

Configuration	R (or h_p)
Corner (C)	
$(\phi_W + \phi_B < 3\pi/2)$	$R = \sqrt{\frac{2V}{3\pi/2+2\cos\phi_W\cos\phi_B+\cos\phi_W\sin\phi_W+\cos\phi_B\sin\phi_B-\phi_W-\phi_B}}$
$(\phi_W + \phi_B > 3\pi/2)$	$R = -\sqrt{\frac{2V}{3\pi/2+2\cos\phi_W\cos\phi_B+\cos\phi_W\sin\phi_W+\cos\phi_B\sin\phi_B-\phi_W-\phi_B}}$
$(\phi_W + \phi_B = 3\pi/2)$	$R = \infty$
Two-corner (2C)	
$(\phi_W + \phi_B < 3\pi/2)$	$R = \sqrt{\frac{V}{3\pi/2+2\cos\phi_W\cos\phi_B+\cos\phi_W\sin\phi_W+\cos\phi_B\sin\phi_B-\phi_W-\phi_B}}$
$(\phi_W + \phi_B > 3\pi/2)$	$R = -\sqrt{\frac{V}{3\pi/2+2\cos\phi_W\cos\phi_B+\cos\phi_W\sin\phi_W+\cos\phi_B\sin\phi_B-\phi_W-\phi_B}}$
$(\phi_W + \phi_B = 3\pi/2)$	$R = \infty$
Wall (W)	$R = \sqrt{\frac{V}{\pi+\cos\phi_W\sin\phi_W-\phi_W}}$
Base (B)	$R = \sqrt{\frac{V}{\pi+\cos\phi_B\sin\phi_B-\phi_B}}$
Span (S)	$R = \frac{D}{2\cos\phi_W} \quad (V \leqslant V_c)$
	$R = \sqrt{\frac{V-Dh}{\pi-\phi_W+\cos\phi_W\sin\phi_W}} \quad (V > V_c)$
	$h_p = \frac{V}{D} - \frac{D}{8\cos^2\phi_W}(\pi - 2\phi_W - \sin 2\phi_W), \quad \lim_{\phi_W\to\pi/2} h_p = \frac{V}{D} \quad (V \leqslant V_c)$
Free (F)	$R = \sqrt{V/\pi}$

The usual convention is adopted here of taking R positive if the surface is convex when viewed from outside the phase of interest (the void in this model). For the special case of a span configuration, the height h_p of the meniscus above the base determines the value of A_{WG}.

sessile drop (void) on a rigid substrate. And for the latter situation, one may demonstrate, using variational principles to minimize the free energy, that the liquid/gas interface must assume the shape of a portion of a sphere when gravity is neglected.

Using these assumptions, one may readily obtain expressions analogous to those in Tables 1 and 2 for the 3-D model system. However, two additional configurations are possible in 3-D besides those identified already for 2-D. These are (1) the void situated along an edge between the base and a wall (denoted E_{BW}) and (2) the void situated along the edge between two walls (denoted E_{WW}). The results are given in Tables 3 and 4. The geometric restrictions on the 3-D void in a tetragonal cavity are virtually identical to those for the 2-D system described earlier, and will not be enumerated here.

Table 3
The area of each type of interface as a function of R and ϕ_B for each 3-D void configuration possible in a tetragonal cavity when $\phi_W = \pi/2$

Configuration	A_{BG}	A_{WG}	A_{LG}
Corner (C)	$\frac{\pi}{4}R^2\sin^2\phi_B$	$R^2(\pi + \cos\phi_B \sin\phi_B - \phi_B)$	$\frac{\pi}{2}R^2(1+\cos\phi_B)$
Base/wall edge (E_{BW})	$\frac{\pi}{2}R^2\sin^2\phi_B$	$\pi R^2 - \frac{\pi}{2}R^2(2\phi_B - \sin 2\phi_B)$	$\pi R^2(1+\cos\phi_B)$
Wall/wall edge (E_{WW})	0	πR^2	πR^2
Wall (W)	0	πR^2	$2\pi R^2$
Base (B)	$\pi R^2\sin^2\phi_B$	0	$2\pi R^2(1+\cos\phi_B)$
Span (S)			
$V \leqslant V_c$	D^2	$4Dh_p$	D^2
$V > V_c$	D^2	$4Dh + \pi R^2 - D^2$	$2\pi R^2$
Free (F)	0	0	$4\pi R^2$

For the span configuration, h_p is the height above the base of the triple junction formed at each wall.

Table 4
R as a function of V and ϕ_B for each type of 3-D configuration possible in a tetragonal cavity when $\phi_W = \pi/2$

Configuration	R (or h_p)
Corner (C)	$R = \left[\frac{12V}{\pi(1+\cos\phi_B)^2(2-\cos\phi_B)}\right]^{1/3}$
Base/wall edge (E_{BW})	$R = \left[\frac{3V}{2\pi - \frac{\pi}{2}(1-\cos\phi_B)^2(2+\cos\phi_B)}\right]^{1/3}$
Wall/wall edge (E_{WW})	$R = \left[\frac{3V}{\pi}\right]^{1/3}$
Wall (W)	$R = \left[\frac{3V}{2\pi}\right]^{1/3}$
Base (B)	$R = \left[\frac{3V}{\pi(1+\cos\phi_B)^2(2-\cos\phi_B)}\right]^{1/3}$
Span (S)	$R = \infty \quad (V \leqslant V_c)$
	$R = \left[\frac{3(V-D^2h)}{2\pi}\right]^{1/3} \quad (V > V_c)$
	$h_p = V/D^2 \quad (V \leqslant V_c)$
Free (F)	$R = \left[\frac{3V}{4\pi}\right]^{1/3}$

For the special case of a span configuration, the height h_p of the triple junctions above the base determines the value of A_{WG}.

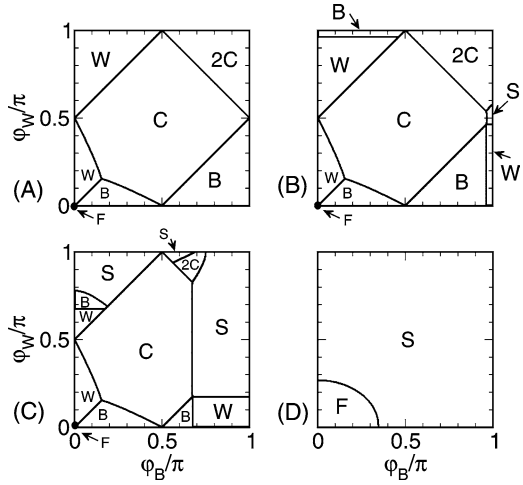

Fig. 4. Isometric cuts of a void stability diagram calculated by the 2-D model for $D = h = 100$ μm ($V_c = 10^4$ μm^2). (A) $V/V_c = 10^{-3}$, (B) $V/V_c = 0.02$, (C) $V/V_c = 0.2$, and (D) $V/V_c = 2.0$.

3. Discussion

3.1. Analysis

In two dimensions, specification of the three constitutive variables (V, ϕ_W, and ϕ_B) and the cavity dimensions D and h is sufficient to determine the thermodynamically favored void configuration consistent with the geometric restrictions. The information can be catalogued conveniently in a "phase diagram" that maps the ranges of constitutive variables within which a given void configuration is stable. Fig. 4 shows four isometric (i.e., constant V/V_c) cuts of such a diagram, using cavity dimensions $D = h = 100$ μm, for which the total cavity volume $V_c = 10^4$ μm^2. The stable configuration in any region is denoted by a single capital letter as shown in Fig. 3. Chatain et al. [1] collect their stability data using the same principle, although in their paper they employ a different set of constitutive variables.

If the dimensions of the cavity are large compared to the dimensions of the void, then none but the span configuration are geometrically constrained. Therefore, the stability diagram shown in Fig. 4A, where $V/V_c \to 0$, is determined only by the minimization of the free energy at constant volume. The symmetry of Fig. 4A therefore is expected because, from the perspective of the void, the cavity is essentially a single corner with base and wall extending away from it indefinitely. When the cavity dimensions are more comparable to the void dimensions, the base, wall, or corner configurations can become geometrically impossible, especially at larger values of ϕ_W or ϕ_B for which the void becomes extremely anisometric. This is reflected in Figs. 4B–4D. The broken symmetry in Figs. 4B and 4C is also due partially to the fact that the cavity itself is asymmetric, being open at the top but bounded on the bottom and sides.

To be more quantitative about the changes that occur at increasing void volumes, notice in Fig. 4B that regions of stability for the base and wall configurations appear in narrow bands for which ϕ_W or ϕ_B exceed critical values ϕ_W^c or ϕ_B^c, respectively. Both ϕ_W^c and ϕ_B^c decrease from a maximum value of π as the void volume increases. To see why this is, take as an example the base configuration. A value of $\phi_B = \pi$ means that a void in contact with the base will spread indefinitely, but because the walls limit the extent of spreading, the base configuration is geometrically impossible for

$\phi_B = \pi$ at any finite volume. For very small void volumes, $V/V_c < 0.01$ the value of the critical angles are sufficiently close to π that the new stability regions, although present, are not visually discernible in Fig. 4A.

We can approximate these critical angles as a function of volume. For example, by explicitly writing the constraint in Eq. (C.13), with R taken from Table 2, the value of ϕ_B^c will be that for which

$$4V \sin^2 \phi_B^c = D^2\left(\pi + \cos\phi_B^c \sin\phi_B^c - \phi_B^c\right). \tag{6}$$

If we use $\alpha = \pi - \phi_B^c$ as a variable, then for $\alpha \to 0$ we can expand Eq. (6) to second order and solve to find

$$\phi_B^c \approx \pi - \frac{8V}{D^2} \quad \left(\pi - \phi_B^c \ll 1\right). \tag{7}$$

Another change in the stability diagrams at larger void volumes is the appearance of a region near the point ($\phi_W = \pi/2$, $\phi_B = \pi$) in which a span configuration is favored. Again, when $\phi_B \to \pi$ a base configuration is not possible because the void would spread indefinitely, leading to a span configuration. However, the span configuration is only possible, at small void volumes, if the meniscus is a flat line in 2-D (a plane in 3-D). If the meniscus is convex or concave, then it is geometrically impossible to enclose a sufficiently small volume under such a meniscus that spans the cavity. But as long as the meniscus is flat or nearly so (i.e., $\phi_W \approx \pi/2$) then any void volume can be contained by adjusting the height of the meniscus above the base surface. The range of ϕ_W over which the span configuration is favored, when $\phi_B = \pi$, can be estimated by following the same procedure as that leading to Eq. (7). The result is written compactly as

$$\left|\frac{\pi}{2} - \phi_W^c\right| \approx \frac{8V}{D^2} \quad \left(\phi_B = \pi,\ |\pi/2 - \phi_W| \ll 1\right). \tag{8}$$

As shown in the upper right corner of Fig. 4B, the C and 2C configurations have equal free energies along the boundary defined by $\phi_W + \phi_B = 3\pi/2$. It is exactly this condition for which the liquid–gas interface has zero curvature. As shown in Appendix B, when the liquid–gas interface has zero curvature, the free energy of N voids, having total volume V, in corner configurations is independent of N and there is no driving force either for coarsening of the voids or for anticoarsening. This result agrees with previous results by Chatain et al. [1].

For the 3-D model, Fig. 5 shows plots of $\Gamma - \Gamma_{\text{free}}$ vs ϕ_B for two different void volumes. The new "edge" configurations available in 3-D are in no case the most stable. With the exception of these two configurations, we can directly compare the results of Fig. 5 to the 2-D model. To make that comparison as meaningful as possible, we first normalize the free energy of each configuration, in 2-D and 3-D, by the free energy of a free void. The result is a set of dimensionless functions α_{i2} and α_{i3} in two and three dimensions, respectively, for configuration i. These functions each have range [0, 1]. Furthermore, recalling that the 3-D model in its present form is valid only for $\phi_W = \pi/2$, we will assume this

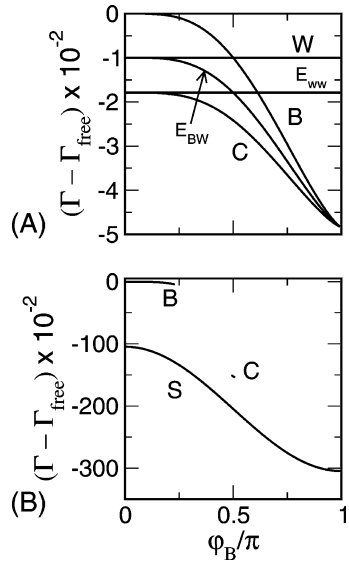

Fig. 5. Free energies calculated by the 3-D model of each configuration when $D = h = 100$ μm. (A) $V/V_c = 10^{-3}$ and (B) $V/V_c = 0.5$. For both plots, $\phi_W = \pi/2$, and the terminating points of some of the curves indicate the range over which a given configuration can satisfy its geometric constraints imposed by the cavity dimensions.

value for the 2-D model as well. Fig. 6 plots these normalized functions for corner, wall, and base configurations. The additional edge configurations available in the 3-D model are omitted from the figure for clarity. For every configuration, the values for the 3-D model differ from those of the 2-D model by no more than 15%. Therefore, we may have confidence that the 2-D model is sufficient for giving qualitatively meaningful insights and predictions.

3.2. Application

Stability diagrams like those in Fig. 4 can predict the equilibrium morphology of voids in a given system, and they also can address the more practical question of how the constitutive variables must be changed to reduce the stability of a trapped void. A striking prediction from Fig. 4A is that very small voids are stable only when the liquid perfectly wets both surfaces. If the practical objective is to eliminate all voids, regardless of their size, then either work must be supplied or the liquid and/or solids must be modified to promote perfect wetting. In many practical systems involving combinations of organic and metallic surfaces, perfect wetting may be a difficult task because these solid/vapor surfaces often have low surface energy densities and therefore are difficult to wet.

When it is not feasible to eliminate the possibility of void formation, it is natural to ask (1) how much work must be performed to free a void, and (2) whether there are other methods of introducing the liquid, instead of rapid immersion, that are less likely to form a void in the first place. The first question will be addressed here; the latter question is outside the scope of the paper.

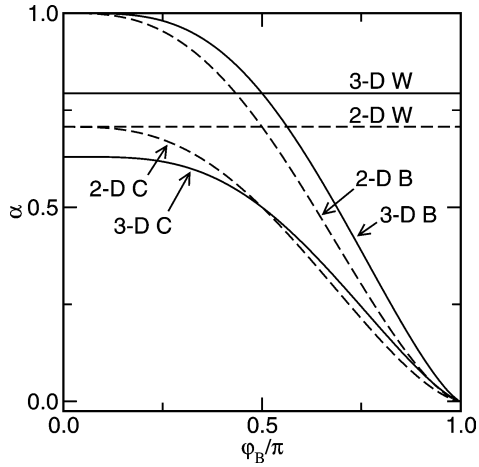

Fig. 6. Normalized free energies $\alpha = \Gamma/\Gamma_{\text{free}}$ for various configurations predicted by the restricted 3-D model (solid curves) and by the 2-D model (dashed curves) for voids with $V/V_c = 10^{-3}$.

By examining results like those in Fig. 5, we may calculate the work required to liberate a void of a given configuration. As mentioned earlier, a free void cannot be thermodynamically favored under these conditions. However, as Fig. 5 shows, any reduction in the contact angle between the liquid and the walls (or, in fact, the base) will reduce the work required to free a void. Noting the difference in vertical scale between Figs. 5A and 5B, the plots also confirm the intuitive notion that more work is required to liberate a void as its volume increases.

Work added to the system allows it to sample higher free energy states and therefore increases the likelihood of forming a free void. Once formed, a free void is unstable toward rising to the top of the liquid under buoyancy forces, but this will occur only if a path is available for the void to rise. Otherwise, the free void is more likely to reform in a trapped configuration of lower free energy.

We close this section with a few comments on the applicability of the model to real systems. Obviously, during the formation of a void, the system will often be far from equilibrium and hydrodynamic factors will play an important role in determining the initial configuration. More importantly, the initial configuration may be metastable relative to the configuration indicated in the diagram for the appropriate values of ϕ_W and ϕ_B. As an example, Fig. 4D indicates that, for void volumes that are large relative to the cavity volume, a liberated void is the only stable configuration if both ϕ_W and ϕ_B are sufficiently small. However, it may be likely for hydrodynamic reasons that a span configuration would form initially, making a bubble that spans the opening of the cavity. The span configuration has higher free energy than a free void when both wetting angles are small. But in the span configuration, the meniscus capping the cavity could adopt a local equilibrium shape, and transporting liquid to the base surface to liberate the void would undoubtedly require a supply of work in some form. Therefore, as with the application of any equilibrium analysis, one must be wary of metastable states.

We also may use this model to infer the behavior of voids at other types of rough surfaces. First, it is more common in practical situations for the surface to be more chemically homogeneous than is assumed by this model. Simply setting $\phi_W = \phi_B$ will make the analysis here applicable to systems such as an embossed metal or the inside of a syringe.

The present model also may be extended to surfaces for which the "base" and "wall" are not mutually orthogonal. For such systems, the free energies of the wall, base, and free configurations at equilibrium must be basically unchanged by departures from orthogonality. The geometric limits of stability will be different, but even these changes should be small when the deviation from orthogonality is not too severe. On the other hand, the corner configuration should become increasingly less stable as the interior angle, θ, between the wall and base becomes more oblique. In the limiting case where the $\theta \to \pi$, i.e., the wall and base are coplanar, it is not possible for the liquid–gas surface to meet both types of surfaces while retaining constant mean curvature unless $\phi_W = \phi_B$. Thus equilibrium is impossible and the void will spontaneously migrate to the surface for which the contact angle is greater. Based on these considerations, the stability of a void is expected to be influenced increasingly by the least wetting surface as θ becomes more oblique. For the same reasons, the corner configuration should become increasingly favorable as θ becomes more acute.

4. Conclusions

A relatively simple 2-D model has been developed to understand the thermodynamic stability of voids trapped at liquid–solid surfaces. It is important to note that this paper does not address mechanisms of void formation, which undoubtedly involve complex hydrodynamic factors at the liquid–solid interface. Also, the model does not address the kinetics of void liberation, which will be dependent on factors such as the rheological properties of the liquid and the temperature. An understanding of the mechanisms both of void formation and of void removal are necessary to predict the likelihood and density of void-like defects and for prescribing detailed methods by which voids can be removed. Nevertheless, the kind of analysis presented here can provide useful insights into the energetics of the problem and can suggest promising directions for making further progress in the study of such systems.

Acknowledgments

Edwin Fuller is gratefully acknowledged for a critical review of the manuscript. The author is also indebted to Ellen Siem and W. Craig Carter for their valuable comments.

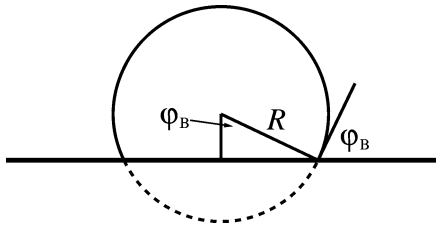

Fig. 7. 2-D geometry for a base configuration used in deriving the areas, A_{ij} of the various interfaces and the radius, R, as a function of volume.

Appendix A. Example derivations

The functions in Tables 1–4 were derived using simple mensuration formulas for circles in 2-D or spheres in 3-D. The mensuration formulas can be derived easily or found in reference books (for example, see Ref. [9]). As an example of the procedure, the results for the functions $A_{ij}(R)$ and $R(V)$ are derived for the 2-D base configuration.

In the base configuration, the area of the interface between the void and the wall surface, A_{WG}, is zero by definition. The area of the interface between the void, having radius R, and the base surface, A_{BG}, is twice the length of the lower leg of the triangle shown in Fig. 7:

$$A_{\mathrm{BG}} = 2R\sin\phi_{\mathrm{B}}. \tag{A.1}$$

The area of the interface between the void (radius R) and the liquid, A_{LG}, is the difference between the perimeter of the circle and the arc length of the imaginary cap that lies below the base (see Fig. 7):

$$A_{\mathrm{LG}} = 2\pi R - 2R\phi_{\mathrm{B}}. \tag{A.2}$$

The volume of a void of radius R in the base configuration is the difference between the volume of a circle of radius R and the volume of the imaginary cap that lies below the base (see Fig. 7):

$$V(R) = \pi R^2 - R^2(\pi + \cos\phi_{\mathrm{B}}\sin\phi_{\mathrm{B}} - \phi_{\mathrm{B}}). \tag{A.3}$$

Solving for R produces

$$R = \tilde{R}(V) = \sqrt{\frac{V}{\pi + \cos\phi_{\mathrm{B}}\sin\phi_{\mathrm{B}} - \phi_{\mathrm{B}}}}. \tag{A.4}$$

Appendix B. Multiple voids

We wish to determine conditions for which, given a fixed gas volume, a multiple number of smaller voids may have lower free energy than a single void in at least one of the configurations shown in Fig. 3.

Let there be N voids, all having the same configuration[3] but arbitrary volumes, and let $v(R)$ be the fraction of the total volume V occupied by any one of these voids having liquid–gas interface radius R. Furthermore, let $\rho(v)$ be the number of voids having volumes between vV and $(v+dv)V$, such that

$$\int_0^1 \rho(v)\,dv = N. \tag{B.1}$$

The radius of the liquid–gas interface for any void having volume vV is

$$R(v) = v^{1/d}R \tag{B.2}$$

and the interfaces have areas following the form

$$A_{pq}(v) = v^{1-1/d}A_{pq,1}, \tag{B.3}$$

where $A_{pq}(v)$ is the area of the interface between phases p and q for a void with volume vV and $A_{pq,1}$ is the analogous quantity for a single void of the same configuration having the same total volume as the N-void system. Therefore, the total area of each type of interface bounding the voids in the N-void system is

$$A_{pq,1}\int_0^1 \rho(v)v^{1-1/d}\,dv = A_{pq,1}N\langle v^{1-1/d}\rangle, \tag{B.4}$$

where $\langle v^{1-1/d}\rangle$ is the arithmetic mean value of $v^{1-1/d}$. This relation holds for the area of all the types of interface, so

$$\frac{\Gamma^{\mathrm{tot}}}{\Gamma} = N\langle v^{1-1/d}\rangle. \tag{B.5}$$

Now, because $\langle v\rangle \equiv 1/N$ and $v < 1$, we have

$$\langle v^{1-1/d}\rangle > \frac{1}{N} \quad (N > 1). \tag{B.6}$$

Substituting into Eq. (B.5) gives

$$\frac{\Gamma^{\mathrm{tot}}}{\Gamma} > 1. \tag{B.7}$$

If $\phi_{\mathrm{W}} \leqslant \pi/2$ and $\phi_{\mathrm{B}} \leqslant \pi/2$, then these results indicate that Γ of an N-void system having a single type of configuration exceeds that of a single void with the same configuration and total volume. Furthermore, for a wall, base, or free configuration, *regardless* of the values of ϕ_{W} and ϕ_{B}, the area of the liquid–gas interface at constant volume increases with number of voids. Therefore, the free energy for all of these three configurations is minimized for a single void. However, the situation is more complicated for the corner configuration if $\phi_{\mathrm{W}} + \phi_{\mathrm{B}} > 3\pi/2$, because all three types of interface are present and Γ *decreases* with increasing A_{BG} (because $\cos\phi_{\mathrm{B}} < 0$) and A_{WG} (because $\cos\phi_{\mathrm{W}} < 0$).

For simplicity in analyzing the corner configuration when $\phi_{\mathrm{W}} + \phi_{\mathrm{B}} > 3\pi/2$, we assume that all N voids have the same volume.[4] Substituting the 2-D results from Table 1 into

[3] The span configuration is not considered because there can only be one void of that type.

[4] Actually $N = 1$ or 2 for the corner configuration because there are only two corners available in the model. Nevertheless, it seems desirable to keep the arguments as general as possible.

Eq. (5) and differentiating with respect to N gives

$$\frac{d\Gamma}{dN} = \frac{\partial\Gamma}{\partial N} + \frac{\partial\Gamma}{\partial R}\frac{\partial R}{\partial N} = \pm\left[\frac{V}{2N}\left(\frac{3\pi}{2} + 2\cos\phi_W\cos\phi_B + \cos\phi_B\sin\phi_B + \cos\phi_W\sin\phi_W - \phi_W - \phi_B\right)\right]^{1/2}, \tag{B.8}$$

where the expression for R from Table 2 has been substituted into the final result. The negative root applies only if the center of curvature of the interface is outside the void ($\phi_B + \phi_W > 3\pi/2$). Therefore, Eq. (B.8) shows that, neglecting other geometric constraints, the free energy of the 2C configuration is actually less than that for the C configuration only if $\phi_B + \phi_W > 3\pi/2$. Note that if $\phi_B + \phi_W = 3\pi/2$, then the liquid–gas interface is flat, the collection of terms in parentheses in Eq. (B.8) sums to zero, and therefore the C and 2C configurations have the same free energy. Finally, it also can be shown, using the same principles as in preceding paragraphs, that the 2C configuration has minimum free energy when both voids have the same volume.

So far, we have not addressed the case for which, in an N-void system, the voids adopt different configurations. But any void in an N-void system, if not already in the stable configuration for its values of ϕ_W and ϕ_B, can only lower its free energy by isometrically transforming to the stable configuration. This means that a system of N voids in different configurations has higher free energy than the same N voids all in the stable configuration. Therefore, the configurations considered in this paper (see Fig. 3) are the only ones eligible to have the minimum free energy.

Appendix C. Geometric constraints on 2-D voids

We catalogue here the conditions for which a 2-D void of a given configuration is geometrically allowable. If one or more of the conditions for a particular configuration is violated, then that configuration is disallowed even if it would have the minimum free energy.

C.1. Corner (C)

$$R < \frac{D}{1+\cos\phi_W} \quad (\phi_B \geqslant \pi/2), \tag{C.1}$$

$$R < \frac{D}{\sin\phi_B + \cos\phi_W} \quad (\phi_B < \pi/2), \tag{C.2}$$

$$\phi_B + \frac{\pi}{2} > \phi_W, \tag{C.3}$$

$$\phi_W + \frac{\pi}{2} > \phi_B. \tag{C.4}$$

If either of the first two constraints is not met, then the void is so large that only a span configuration is geometrically possible. If either the third or fourth condition is not met, then no portion of a circle can simultaneously meet the wall and base at the required contact angles.

C.2. Void at each corner (2C)

$$2R < \frac{D}{1+\cos\phi_W} \quad (\phi_B \geqslant \pi/2), \tag{C.5}$$

$$2R < \frac{D}{\sin\phi_B + \cos\phi_W} \quad (\phi_B < \pi/2), \tag{C.6}$$

$$\phi_B + \frac{\pi}{2} > \phi_W, \tag{C.7}$$

$$\phi_W + \frac{\pi}{2} > \phi_B. \tag{C.8}$$

C.3. Wall (W)

$$2R\sin\phi_W \leqslant h \quad (\phi_W \geqslant \pi/2), \tag{C.9}$$

$$R(1+\sin\phi_W) < h \quad (\phi_W < \pi/2), \tag{C.10}$$

$$R(1+\cos\phi_W) < D. \tag{C.11}$$

C.4. Base (B)

$$2R < D \quad (\phi_B < \pi/2), \tag{C.12}$$

$$2R\sin\phi_B < D \quad (\phi_B \geqslant \pi/2). \tag{C.13}$$

C.5. Span (S)

$$h_p > 0 \quad (\phi_W \leqslant \pi/2), \tag{C.14}$$

$$h_p + \frac{D}{2\cos\phi_W}(1-\sin\phi_W) > 0 \quad (\phi_W > \pi/2), \tag{C.15}$$

where h_p is given in Table 2.

References

[1] D. Chatain, P. Wynblatt, S. Hagege, E. Siem, W. Carter, Interface Sci. 9 (2001) 191.
[2] J. Gibbs, The Collected Works of J. Willard Gibbs, vol. 1, Thermodynamics, Yale Univ. Press, New Haven, CT, 1928.
[3] W. Winterbottom, Acta Metall. 15 (1967) 303.
[4] R. Collins, J.C.E. Cooke, Trans. Faraday Soc. 55 (1959) 1602.
[5] M. Erle, D. Dyson, N. Morrow, Am. Inst. Chem. Eng. J. 17 (1) (1971) 115.
[6] W. Carter, Acta Metall. 36 (8) (1988) 2283.
[7] J. Bullard, M. Menon, J. Colloid Interface Sci. 219 (1999) 320.
[8] J. Howe, Interfaces in Materials, Wiley, New York, 1997, p. 178.
[9] W. Beyer (Ed.), CRC Standard Mathematical Tables, 27th ed., CRC Press, Boca Raton, FL, 1984.